

Article

Thermodynamics of Micelle Formation and Membrane Fusion Modulate Antimicrobial Lipopeptide Activity

Dejun Lin¹ and Alan Grossfield^{1,*}

¹Department of Biochemistry and Biophysics, University of Rochester Medical Center, Rochester, New York

ABSTRACT Antimicrobial lipopeptides (AMLPs) are antimicrobial drug candidates that preferentially target microbial membranes. One class of AMLPs, composed of cationic tetrapeptides attached to an acyl chain, have minimal inhibitory concentrations in the micromolar range against a range of bacteria and fungi. Previously, we used coarse-grained molecular dynamics simulations and free energy methods to study the thermodynamics of their interaction with membranes in their monomeric state. Here, we extended the study to the biologically relevant micellar state, using, to our knowledge, a novel reaction coordinate based on hydrophobic contacts. Using umbrella sampling along this reaction coordinate, we identified the critical transition states when micelles insert into membranes. The results indicate that the binding of these AMLP micelles to membranes is thermodynamically favorable, but in contrast to the monomeric case, there are significant free energy barriers. The height of these free energy barriers depends on the membrane composition, suggesting that the AMLPs' ability to selectively target bacterial membranes may be as much kinetic as thermodynamic. This mechanism highlights the importance of considering oligomeric state in solution as criterion when optimizing peptides or lipopeptides as antibiotic leads.

INTRODUCTION

The pressing need for novel antibiotics against resistant strains of bacteria and fungi has become a global medical concern. An emerging class of antimicrobial drug candidates, antimicrobial peptides (AMPs), has been the focus of significant research on antiresistance antibiotics (1). Unlike traditional antibiotics that target specific growth or function processes of the microbes, many AMPs were found to disrupt the structure and function of their membranes (2). AMPs' lipophilicity endows them with a few advantages as antimicrobial drugs. Membrane composition is relatively conserved during evolution, which makes AMPs less vulnerable to evolved resistance than traditional antibiotics. Moreover, AMPs' membrane binding mechanism shields them from several resistance strategies, such as multidrug efflux transporters (3,4).

However, there are also disadvantages that limit AMPs' clinical application. One of the major hurdles is that they are expensive to manufacture, process, and store because they are much larger and chemically complex than typical drug molecules (5,6). This is in part because there appears to be a lower limit to the size of traditional AMPs; they must be hydrophobic enough to bind membranes stably, and thus must have a significant number of hydrophobic side chains to overcome the polarity of the peptide backbone. Additional residues, often cationic, are usually required to make the peptides selective for anionic bacteria-like membranes. The result is that most natural AMPs

are 12–40 amino acids long, far larger than most druglike molecules.

Another major obstacle to AMPs' application is the lack of understanding the relation between their oligomerization in solution and their biological activity. Some AMP oligomers are associated with improved peptidase resistance (7,8) and enhanced cell selectivity (7,9–14) compared to their monomers. While the former can be understood as the consequence of structural changes upon oligomerization or exclusion from degrading enzymes' active sites, the reason for the latter remains a mystery. Although the microbial membranes are believed to be the major targets of AMPs, one cannot rule out the possibility that other cell surface structures could affect the membrane activity of AMPs. In fact, it was surmised that the preassembled AMPs might be retained by macromolecules on cell surfaces and kept from interacting with membranes simply because of their increased sizes compared to monomers (11,14). Unfortunately, the limited resolution from experiments and the lack of molecular insights make it hard to explain why this kind of blockage would only occur for certain microbial species with specific AMPs, as opposed to being a universal phenomenon. One could attempt to examine the impact of AMP oligomerization on membrane binding by simply introducing more hydrophobic amino acids to increase the propensity to form oligomers, but this approach would also alter the structure of the individual molecules, and likely the membrane interaction as well. Alternatively, one could covalently link the monomers together (14), but this approach would significantly increase the cost of AMP manufacturing; moreover, the choice of linkage would

Submitted April 16, 2015, and accepted for publication July 1, 2015.

*Correspondence: alan_grossfield@urmc.rochester.edu

Editor: Markus Deserno

© 2015 by the Biophysical Society
0006-3495/15/08/0750/10

<http://dx.doi.org/10.1016/j.bpj.2015.07.011>



almost certainly affect the nature of the membrane-bound state.

All the aforementioned complexities complicate the efforts to optimize their performance. For example, in typical virtual screening studies where AMPs' activity is modeled based on their primary sequences, the large amount of training data required to build an accurate model is practically impossible to obtain for large peptides due to the limit in generating high-throughput screening arrays, where the number of array elements scales exponentially with the peptide length (15). Also, peptides tend to be flexible, with a broad range of accessible conformations; this can significantly complicate the interpretation of mutagenesis data, as even seemingly simple substitutions can significantly alter the peptides' conformation and pose relative to the membrane. This flexibility also makes AMPs challenging targets for computer simulation; their structural plasticity combined with the slow relaxation times for lipid-peptide interactions make it very hard to acquire adequate statistical sampling, even using state-of-the-art enhanced sampling methods (16,17). For these reasons, as well as their susceptibility to protease degradation *in vivo* and their potential toxicity to human cells (5), there has been only limited success in making AMPs into internal antibiotics (15).

In an attempt to bypass the specific issues of AMPs, Avrahami and Shai (18,19) devised an alternative approach to utilize AMPs' membrane activity by conjugating fatty acids to short cationic peptides. These small synthetic molecules, called antimicrobial lipopeptides (AMLPs), mimic AMPs' amphipathicity and cationic nature, and have been shown to be potent antimicrobials with minimal inhibitory concentrations in the micromolar range. Based on a more recent design of AMLP scaffold, C16-KXXX, where "C16-" denotes the palmitoyl chain attached to the N-terminus of the tetrapeptide KXXX containing two lysines and two guest residues X, Makovitzki et al. (20) found several potent antimicrobials that had insignificant hemolysis. Later work further showed that similar AMLPs were able to clear infections *in vivo* (21). Most notably, C16-KGGK (the bold letter denotes the D-enantiomer, included to confer resistance to peptidase degradation (22)), the most potent among these AMLPs, has a micromolar MIC against several pathogenic microbes, including both bacteria and fungi. The attachment of the acyl chains to peptides also promoted their aggregation (23), making these lipopeptides excellent models for studying oligomerization.

Most of the experimental work on these AMLPs to date focused on their efficacy on a macro- or mesoscopic scale, so relatively little is known about their mechanisms at the level of individual molecules. To better understand AMLPs' mode of action, our lab has been using a combination of all-atom and coarse-grained (CG) molecular dynamics (MD) simulations to examine these lipopeptides' membrane activity. While all-atom simulations provide atomic details about the membrane perturbation caused by AMLPs (24),

it is prohibitively expensive to quantitatively measure the thermodynamics of membrane binding. We thus used a CG model to examine slow processes such as AMLPs' binding to membranes (25,26). The CG model we used, the MARTINI force field, is designed such that each CG particle represents four heavy atoms; it generally runs at least two orders of magnitude faster than an equivalent all-atom model (27,28) and is able to reproduce experimental results in many cases (29–34).

Our previous simulations using the MARTINI model quantified the binding thermodynamics of monomeric C16-KGGK to membranes (26). Our results indicated that the acyl chain of these AMLPs dominates their binding affinity to membranes, while the peptide portion confers selectivity for anionic membranes (26). However, both experiments (23) and simulations (24,25) suggested that these AMLPs tend to aggregate into nanostructures at moderate concentrations; such aggregates are thought to enhance AMLPs' solubility and antimicrobial activity and could contribute to their resistance to degradation. Thus, the focus of this work is to study the interactions between larger aggregates (micelles) of AMLPs and membranes.

However, there are technical difficulties regarding the simulation of amphiphile aggregation. Aggregates of even moderate size tend to be at least metastable, so obtaining a well-equilibrated size distribution is very challenging, requiring either very long simulations or efficient enhanced sampling algorithms. For example, an analogous process, vesicle fusion, takes place in milliseconds to hundreds of microseconds, which is extremely challenging to simulate using brute-force methods (35), even with a CG force field. To explore the process of AMLPs binding to membranes by brute-force means, we would need to consider the transfer of any AMLP from one aggregate to another as well as from an aggregate to membrane. These transitions are very slow, because they require partial exposure of the hydrophobic tails to water (26).

In this study, we introduce, to our knowledge, a novel reaction coordinate, the hydrophobic contact number, that characterizes the aggregation of amphiphiles and their binding to membranes. Using umbrella sampling along this reaction coordinate, we calculated the free energy of the formation of a C16-KGGK micelle in water and the binding of this micelle to membranes. Our results show that this micelle has much higher affinity to the anionic bacterial-like membrane than the neutral mammalian-like membrane, consistent with our previous results on the monomeric C16-KGGK (26). Most surprisingly, these calculations revealed a significant free energy barrier to micelle membrane entry, which was absent in the monomeric C16-KGGK case. This barrier is much higher in the case of the zwitterionic mammalian-like membrane than the anionic bacterial-like membrane, which means the binding to the latter is more favorable not just thermodynamically but kinetically as well. Our analysis reveals that the mechanisms of micelle

membrane entry depend on the membrane compositions, which explains the variation in the barrier. The results suggest a link between the stability of the lipopeptide micelles and their membrane selectivity and provide biophysical insight into antimicrobial drug optimization based on AMLPs.

MATERIALS AND METHODS

System construction

All systems were modeled using the MARTINI coarse-grained force field, Vers. 2.2P (36,37). We used two lipid bilayer compositions: a 2:1 mixture of POPE (1-palmitoyl-2-oleoyl-sn-glycero-3-phosphoethanolamine) and POPG (1-palmitoyl-2-oleoyl-sn-glycero-3-phosphoglycerol), representing a Gram-negative bacteria-like membrane, and pure POPC (1-palmitoyl-2-oleoyl-sn-glycero-3-phosphocholine), representing a mammal-like membrane. Construction of the membrane bilayers was described previously in Horn et al. (25). Each system contained 480 lipids (240 per leaflet), and care was taken to ensure both leaflets had the same composition. Hydration was modeled using the polarizable MARTINI water model (36).

The C16-KGGK molecule was constructed by merging the MARTINI palmitoyl with the MARTINI KGGK peptide. The MARTINI model does not have sufficient resolution to represent chirality, but this is not a serious limitation: a four-residue peptide is too short to form secondary structure, and in any event, experiments show that varying the backbone chirality has no significant effect on the lipopeptide's properties (38). For the purposes of the MARTINI model, we treated these peptides as random coil, and did not apply any secondary structure restraints. A box of water with randomly scattered C16-KGGKs was equilibrated for several hundred nanoseconds until the C16-KGGKs aggregated into micelles. We extracted the largest of these micelles and removed several lipopeptides to produce a 48-mer; binding a single 48-lipopeptide micelle to either membrane composition produces a 10:1 lipid/peptide.

For each bilayer composition, we placed the C16-KGGK micelle ~60 Å from the bilayer center of mass. The system was then solvated with water, and sodium and chloride ions were added to reach a concentration of ~100 mM. Extra counterions were added to neutralize the charges on lipids and lipopeptides. The membrane binding simulations contained a total of 51,300 CG particles, while the simulations of micelle formation in water contained 12,730 particles.

Umbrella sampling

The potentials of mean force (PMF) to bind a C16-KGGK micelle to a lipid bilayer were calculated using umbrella sampling and the weighted histogram analysis method (WHAM) (39). The reaction coordinates (RCs) we used were based on the number of hydrophobic contacts within the micelle and between the micelle and the membrane; the reasons using these RCs (in place of more common choices, such as the distance from the membrane center) are discussed in Section S1.1 in the [Supporting Material](#).

Specifically, the number of contacts between a pair of molecules i and j is defined as a smooth function of the distance between their centers-of-mass distance r_{ij} ,

$$S_{ij}(r_{ij}) = \frac{1}{1 + (r_{ij}/r_0)^n} \quad (1)$$

where r_0 is the distance at which the contact is exactly 0.5 and n controls the steepness of the function. The total number of contacts between two groups of particles A and B is the sum of S_{ij} over all the unique pairs between A and B :

$$C_{AB} = \sum_{i \in A} \sum_{j \in B} S_{ij}. \quad (2)$$

Note that in the case of $A = B$, we constrained the sum so that $i \neq j$ and any pair of i and j appears only once in the sum.

To facilitate the computation, we used a neighbor list with a cutoff distance R_{cut} to keep track of the pairs involved in Eq. 2. We chose R_{cut} so that both $S_{ij}(R_{\text{cut}})$ and $dS_{ij}/dr_{ij}(R_{\text{cut}})$ were sufficiently small (see [Table S1](#)). In all cases, the neighbor list was updated every five steps in all the simulations.

The restraint potentials in umbrella sampling are of the form

$$U = \frac{k}{2}(C_{AB} - C_{AB}^0)^2, \quad (3)$$

with C_{AB}^0 being the reference position of each window.

The details of RC definition, the parameters in Eqs. 1–3, and the number of sampling windows are summarized in [Table S1](#). Note that in the membrane binding simulations, we purposely chose to only sample a subset of the range of RCs in [Table S1](#), and the reference positions (C_{AB}^0 in Eq. 3) of all the umbrella sampling windows are plotted in [Fig. S1](#). This range of RCs covers the transformation from the micelle being far away from the membranes to all lipopeptides in the micelle inserted and spread out in the upper leaflet.

The structures used to seed the umbrella sampling windows were generated by steered MD (SMD) simulations, where the equilibrium positions of the harmonic potential in Eq. 3 were moved from a starting position to an ending position at constant velocity. Multiple SMD simulations with different starting and ending positions were used so that the desired range of the reaction coordinate was covered. Snapshots from the SMD simulations were used to seed the umbrella samplings such that the starting RC values were as close to the centers of the window as possible.

Hamiltonian replica exchange

For the micelle formation simulations, Hamiltonian replica exchange (HREX) was used to facilitate the convergence of the umbrella sampling. The umbrella sampling windows were exchanged using a Gibbs sampling algorithm described in Chodera and Shirts (40). The HREX was attempted every 500 steps. In principle, we could have used HREX for the micelle-membrane binding simulations as well, but the very large number of simulation windows used in these calculations (≈ 800) made the procedure unfeasible with our computational resources.

Weighted histogram analysis method

The weighted histogram analysis method (WHAM) (39) was used to calculate the PMFs from the umbrella sampling data. The dynamic range of the PMFs in each system we were dealing with in this study was usually ~ 200 –300 kcal/mol and the number of umbrella sampling windows was ~ 600 –800. Performing WHAM on such a dataset turned out to be quite challenging, and common implementations of WHAM (41) failed to complete the calculation due to numerical instability. Moreover, in some cases the termination condition of WHAM iteration produced un converged solutions even in the case of a relatively small tolerance (10^{-6}). This is due intrinsically to the slower convergence of WHAM iteration, which has been discussed before in Zhu and Hummer (42). To tackle these issues, we implemented an optimized version of WHAM in C++ based on the idea proposed by Zhu and Hummer (42), where the WHAM equations were solved by maximizing the target likelihood function via the Polak-Ribiere conjugate gradient method with Brent's line search (43). A multiple precision library (44) was used in this implementation to achieve numerical stability in WHAM.

Using this implementation of WHAM (45), the PMFs for micelle formation were calculated using 472 bins and a convergence threshold of 10^{-10} . The PMFs of micelle-membrane binding were calculated using a 300×300 grid and a convergence threshold of 10^{-10} .

Minimum free energy paths

From each of the two-dimensional membrane binding PMFs, we used the string method (46) to calculate the minimal free energy paths (MFEPs) in the two-dimensional contact space. In all cases, the string was initially constructed by 200 images or nodes linearly interpolated between the two terminal nodes at the minima corresponding to the respective surface-bound and inserted states. We refer the reader to “PMFs for Membrane Building” and Fig. 2 later in the article for the definition of these states. The forward Euler method was used to propagate the images with a step size of 0.1 in both dimensions. Bicubic interpolation was used to evaluate the numerical gradients at the images at each step. We terminated the calculation if the mean Cartesian distance of the images between two consecutive steps was <0.001 . In some cases, the string fluctuated around an equilibrium with a fluctuation of 0.01 and we simply terminated the calculation and took the final string as our result. Such fluctuation is due to the relatively coarse grid on which the PMFs were calculated where not all the stationary points of underlying continuous PMFs were resolved. Also, the interpolated numerical gradients inevitably introduced some errors. However, we do not think this would affect any of the conclusions in this study because such errors are minuscule.

Simulation protocol

All simulations were performed using GROMACS, Ver. 4.6.3 (47–49) with the modification described in Umbrella Sampling. For the general MD simulation parameters, we used a 20-fs time step, and updated the neighbor list every five steps. Simulations were performed in isothermo-isobaric (NPT) ensemble with Nosé-Hoover temperature coupling (50,51) and the Parrinello-Rahman barostat (52), set to 300 K and 1 bar, respectively. Electrostatics were accounted for using the shift function with a Coulomb cutoff of 12 Å. A shift was used for van der Waals as well, with a switch distance of 9 Å and a cutoff of 12 Å.

Each of the micelle formation umbrella sampling simulations was run for ~500 ns where the first 100 ns were considered equilibration phase, and were excluded from WHAM and any analysis. This totals to 348 μs (500 ns/window × 696 windows) simulation time. The duration of the equilibration phase was determined by gradually excluding N samples from the beginning of the simulations when we ran WHAM, where N increased with a step size of 50 ns. We called the first N samples the equilibration phase when increasing N does not change the corresponding PMFs significantly. The PMFs corresponding to N in the range between 50 and 250 are plotted in Fig. S11. Most of the membrane binding simulations were run for ~1.3 μs and the windows near the transition states (where there is the most structural diversity) were extended to ~3.7 μs, where the first 350 ns were considered equilibration phase and excluded from WHAM and any analysis. The total simulation time is 1626.4 μs and 1434.4 μs, in the respective cases of POPE:POPG and POPC membrane. The dynamics in the MARTINI force field is usually faster than an equivalent all-atom force field because the coarse-graining results in a smoother potential energy surface; other groups have suggested that simulation times should be multiplied by a factor of 4 to compensate (30), but because the focus of this work is thermodynamics rather than kinetics, we believe it is clearer not to do so.

RESULTS

PMFs of micelle formation

The potential of mean force (PMF) for 48 C16-KGGK molecules to aggregate into one micelle is shown in Fig. 1 A. The PMF has three distinct minima, each corresponding to a distinct oligomerization state of the lipopeptides. The first ($x \approx 270$) and second minima ($x \approx 345$) represent a mixture of different sizes of oligomers ranging from 10 to 30 lipopeptides; the third minimum ($x \approx 450$) corresponds to a micelle of 48 lipopeptides. The maximum at smallest RC values ($x \approx 28$) corresponds to dispersed lipopeptides in water. Interestingly, the global minimum is not the 48-mer but most likely the coexistence of a 17- and a

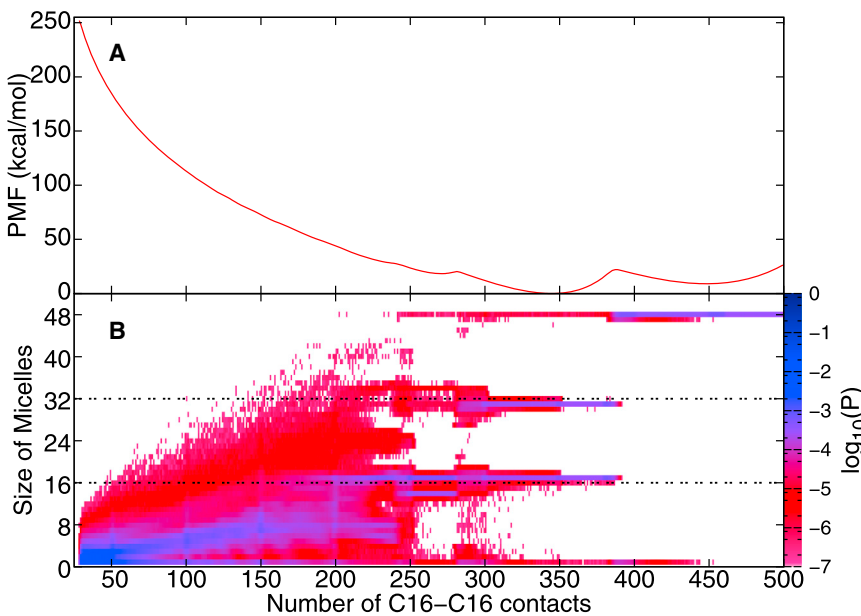


FIGURE 1 (A) PMF in kcal/mol (y axis) as a function of the total number of C16-C16 contacts (x axis, the same as B) between all unique pairs of 48 C16-KGGKs. (B) The joint probability in \log_{10} scale (color box) as a function of the number of C16-C16 contacts (x axis) and the size of lipopeptide clusters (y axis). (Two dashed lines) References to a 32- and a 16-mer, respectively. To see this figure in color, go online.

31-mer (Fig. 1 B) and the free energy barrier to combining the 17- and 31-mer into the 48-mer is ~22 kcal/mol; the 48-mer is metastable by ~9.0 kcal/mol. At least some of this free energy difference is due to the finite size of the simulation cell; each additional lipopeptide added to the micelle removes a lipopeptide from the surrounding bath, artificially increasing the entropic penalty to add the next one (see “C16-KGGK Oligomerization Is Likely To Be Polydisperse” for more details).

Fig. 1 B shows the joint probability of observing a specific lipopeptide micelle/cluster size and the number of hydrophobic contacts formed among the lipopeptides. It is clear that a mixture of lipopeptide micelles/clusters of different sizes dominate the global PMF minima ($x \approx 345$), indicating that the C16-KGGK solution is polydisperse (see C16-KGGK Oligomerization Is Likely To Be Polydisperse for more discussion). It is worth noting that a trace amount of monomers coexists with bigger oligomers near the global minimum as well as the transition to the third minimum (rightmost well in Fig. 1 A).

PMFs for membrane binding

The PMFs for a 48-C16-KGGK micelle binding to a membrane contacts are shown in Fig. 2, A and B. These PMFs are characterized by a surface-bound (Fig. 2, A1 and B1) state and an inserted state (Fig. 2, A3 and B3). These two states are bridged by various transition states (Fig. 2, A2 and B2) residing along a set of saddle points on the PMFs. For reference, we called the case where the micelle is far away from the membrane, corresponding to the upper-right corner of Fig. 2, A and B, the free state.

When the micelle binds to the POPE:POPG membrane, the surface-bound state (Fig. 2 A1) is a local minimum of the PMF (Fig. 2 A), stabilized by the favorable interactions between the POPG phosphates and the lysine side chains in the lipopeptides. In contrast, the equivalent state in the POPC case (Fig. 2 B1) is not metastable (Fig. 2 B); it appears that lysine-phosphate interactions are not strong enough to stabilize surface binding in the absence of anionic headgroups. However, we still refer this state to the surface-bound state for the sake of comparison. The inserted states in both lipids are structurally similar, with the C16 tails of lipopeptides embedded in the membrane hydrophobic core, leaving the KGGK peptides in the membrane-solvent interface.

Aside from the difference in shape, the two PMFs are also distinct from each other in their scales, as shown by the upper limits of the color-bars in Fig. 2, A and B. This is shown more clearly in the PMFs along the MFEPs in Fig. 3, making it evident that binding to the anionic POPE:POPG membrane is far more favorable than binding to POPC.

Moreover, the binding mechanism and transition states differ significantly depending on the membrane composition. When binding to the POPE:POPG membrane, the lip-

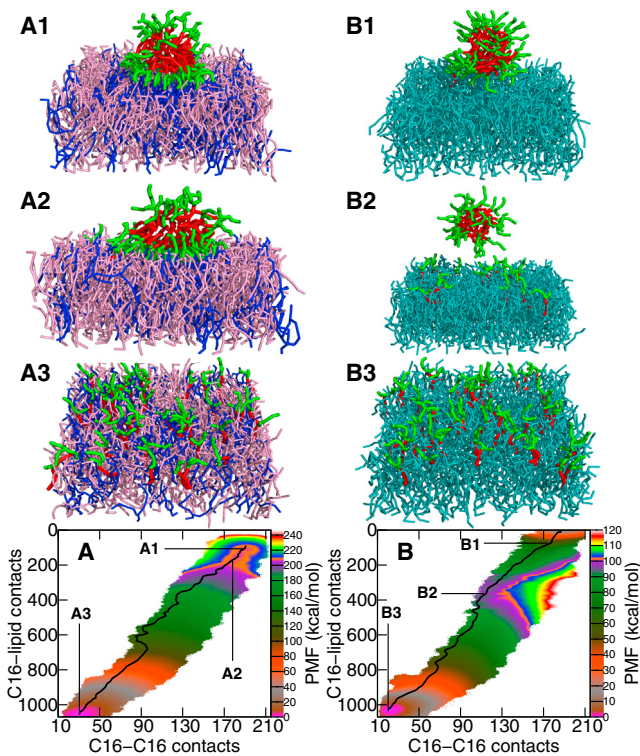


FIGURE 2 The PMFs in kcal/mol (color-scale) of binding a C16-KGGK micelle to either a POPE:POPG (A) or POPC (B) lipid membrane as a function of the number of C16-C16 (x axis) and C16-lipid tail (y axis) contacts (bottom panel). The MFEP was plotted (black line) on the respective PMF. (A1–A3 and B1–B3) States along the minimum free energy path; 1 refers to the surface-associated state, 2 to the transition state, and 3 to the fully inserted state. (Labels and lines) Locations of these states on the PMF (bottom panel). POPC lipids (cyan), POPE (pink), POPG (blue), C16 (red), and KGGK (green). To see this figure in color, go online.

opeptide micelle gets flattened, with the C16 tails stretching out from inside the micelle to the POPE:POPG membrane; this distortion is compensated by strong electrostatic interactions between the lipid phosphates (particularly for PG lipids) and the lysine sidechains. By contrast, the micelle does not tend to stably interact with the surface of the POPC membrane; instead, the lipopeptides are transferred into the POPC membrane one at a time, while the micelle bounces off the surface. The one-at-a-time mechanism is visible in the series of local minima around the labeled transition state in Fig. 2 B, with each local minimum representing a different fraction of lipopeptides transferred from the micelle to the POPC membrane. We will discuss the implications for the mechanism in “Molecular Basis for AMLPs’ Cooperative Binding to Bacterial Membranes”.

MFEPs of membrane binding

The MFEPs of the C16-KGGK micelle binding to membranes and the PMF values along the paths are shown in Figs. 2, A and B, and 3, respectively. The MFEP to bind

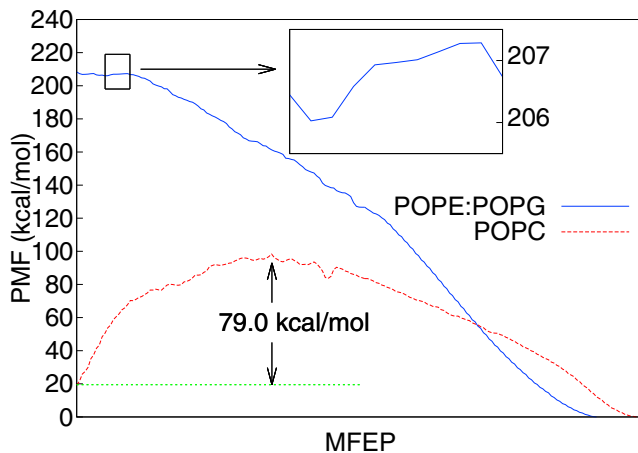


FIGURE 3 PMFs in kcal/mol (y axis) along the MFEP (x axis) as shown in Fig. 2, A and B, of binding a C16-KGGK micelle to either the POPE:POPG (solid line) or POPC (dashed line) lipid membrane. (Inset, the POPE:POPG curve) Transition free energy barrier is \sim 1.3 kcal/mol. The barrier in the POPC case is \sim 79 kcal/mol (labeled by arrows). Note that the path parameters (x axis) of binding to the two different membranes are not comparable, because the number of contacts formed in the bound state varies with membrane composition (see Fig. S4). To see this figure in color, go online.

to the POPE:POPG membrane goes from the surface-bound state to the inserted state with a relatively small transition barrier of 1.3 kcal/mol. In contrast, the MFEP to bind to the POPC membrane encompasses the surface-bound and inserted state, the former of which is part of the transition ensemble. The barrier to making the transition is both very high and broad and peaks at \sim 79 kcal/mol. The locations of the two MFEPs in the two-dimensional contact space are put together in Fig. S4 for comparison.

DISCUSSION

Using free energy calculations and coarse-grained molecular dynamics simulations, we are trying to address the following questions regarding the oligomerization of C16-KGGK and the oligomers' interaction with membranes: 1) what is the equilibrium distribution of different C16-KGGK oligomers, and 2) does oligomerization alter the binding affinity of C16-KGGK to membranes?

C16-KGGK oligomerization is likely to be polydisperse

As shown in Fig. 1, the most likely oligomerization state for 48 C16-KGGK molecules is the formation of a 17- and a 31-mer, with monomers present only occasionally. This configuration is more favorable than the 48-mer micelle (second minimum) by \approx 9.0 kcal/mol. However, this result is altered by the finite size of the simulation cell; as the micelle forms, the concentration of free lipopeptides drops,

which causes the calculation to underestimate the stability of larger aggregates. We propose a simple analytical correction for this issue, discussed in Section S3 in the [Supporting Material](#). When reasonable values for the volumes of the system and individual molecules are plugged in, the correction lowers the free energy of the larger aggregate by \approx 24 kcal/mol relative to the 17-mer/31-mer mix. However, given the significant uncertainties in the correction, we are only able to conclude that both minima are likely thermodynamically accessible. Moreover, these simulations are too small to completely represent mesoscopic structures such as fibrils that were observed experimentally in the case of a similar AMLP (23). Although the precise relative stabilities of different-sized aggregates may be altered by the finite size of the calculation, the umbrella sampling results clearly suggest that the C16-KGGK is most likely polydisperse in solution.

To test the effects of system size on the distribution of oligomers, we also ran three independent simulations of 480 C16-KGGK molecules at the same concentration as in the umbrella sampling ones. The simulations were started from either dispersed monomeric lipopeptides, 48-mers, or a mix of 17- and 31-mers; see Section S4 in the [Supporting Material](#) for more details. The size distribution functions of the C16-KGGK oligomers from these simulations, shown in Fig. S6, show that the two systems starting from the two oligomeric states stayed around their respective minima throughout the simulations, while the one starting from monomers resulted in a mixture of oligomers with sizes ranging from 10 to 38 lipopeptides. This demonstrates that the free energy minima calculated from the umbrella sampling (Fig. 1) are at least metastable, regardless of system size. The population of larger aggregates remains low even in the bigger simulations, and even when they occur, they are not stable. Rather, in these trajectories the large aggregates really just the result of two smaller aggregates momentarily colliding, without actually fusing. This could be a kinetic artifact: medium-sized aggregates do a reasonable job of hiding the acyl chains from solvent, so fusing them requires the same kinds of concerted opening events required for membrane insertion, with significant barriers. Thus, we conclude that 1) the medium-sized aggregates are at least metastable at the concentration studied, 2) larger aggregates are either less favorable thermodynamically or form on much longer timescales, and 3) a solution of C16-KGGK is likely to feature a broad range of aggregate sizes.

Micelles greatly enhance membrane selectivity

Given the broad distribution of oligomer sizes (Figs. 1 and S6), it is not immediately obvious which oligomeric state is most relevant to the membrane activity seen experimentally. In this study, we chose the 48-mer C16-KGGK micelle and a lipopeptide/lipid of 1:10 as our model system

because the expected peptide/lipid in the membrane-bound state of many antimicrobial peptides with micromolar minimal inhibitory concentrations (53) is roughly around this value.

The umbrella sampling results for the 48-mer C16-KGGK micelle binding to membranes show that the micellar state has strong thermodynamic selectivity for anionic membranes; the thermodynamic binding affinity for the model bacterial membrane is much higher than that for the mammalian one, yielding a $\Delta\Delta G_{\text{binding}}$ ($\Delta G_{\text{bacterial}} - \Delta G_{\text{mammalian}} = 246.7 - 19.3 \approx 227.4$ kcal/mol (Fig. 2). Indeed, on a perlipopeptide basis, binding to the model mammalian membrane is ≈ 0.40 kcal/mol, less the $k_B T$, while binding to the model bacterial membrane is favorable by ≈ 5.14 kcal/mol per molecule. This value is much smaller than the one we had measured previously (26) for the isolated lipopeptides using the same model, where binding to the anionic membrane was favorable by -14.5 kcal/mol; the difference reflects the stability of the micelle relative to the monomer in solution.

However, the effect of micellization on binding kinetics is even more striking. Where individual C16-KGGK molecules bind without barrier to both PC and PE:PG membranes (26), micelles experience distinct barriers that depend on the membrane composition. The barrier to entering a POPE:POPG bilayer is relatively small (1.3 kcal/mol), particularly in contrast to the barrier to enter a zwitterionic POPC bilayer (79 kcal/mol). The difference in barrier height is 77.7 kcal/mol, suggesting a difference in binding rates of 10^{56} .

This result helps explain the function of similar lipopeptides *in vivo*, where host membranes will generally be more abundant than bacterial ones. Barrierless binding suggests that isolated lipopeptides will tend to bind strongly ($\Delta G < -10$ kcal/mol) to whatever membrane they encounter first, making it hard to understand how the lipopeptides ever reached their bacterial targets. These results suggest a novel mechanism for selectivity: binding to host mammalian membranes will be slow and inefficient as long as the lipopeptides are micellized in solution, while binding to the bacterial surface will still be efficient. To our knowledge, this favorable aspect of AMLP oligomerization has not been discussed previously in either the experimental or computational literature.

Molecular basis for AMLPs' cooperative binding to bacterial membranes

The cooperative binding of C16-KGGK micelles to the membrane is important for its kinetic selectivity. Because this mechanism has not been explored previously, it is worth examining the molecular-level details of the process, in hopes that we can use the insights to guide rational oligomerization-based optimization.

To quantify structural changes during C16-KGGK's membrane binding, we measured the orientation of the lipopeptide's acyl chains, the size of the lipopeptide micelle/aggregation, the hydration of the lipopeptides, and the lateral radial distribution functions of different lipids in different stages of this process. The details of this analysis and the results are presented in Sections S5.2, S5.3, S5.4, and S5.5 in the *Supporting Material*. As described in Sections S5.2 and S5.5 in the *Supporting Material*, the C16-KGGK micelle initially bound to the bacterial membrane via a surface-bound state stabilized by electrostatic interactions between the peptide side chains and the membrane. These electrostatic interactions were also evident in previous brute-force simulations done by our group (25), as well as the umbrella sampling simulations of monomers binding to membranes (26); these interactions reduce the free energy barrier to binding bacterial membranes relative to zwitterionic ones. This can be understood from two perspectives, as follows.

First, the long-range electrostatics draw the micelle toward the membrane, effectively letting it fall downhill toward the bound state; there is no equivalent interaction with zwitterionic membranes. It is worth noting that these calculations were performed with 100 mM salt, and that this effect would be stronger still in pure water. More interestingly, the micelle altered the lateral structure of the membrane, concentrating the POPG lipids even when the micelle is relatively far away from the membrane (Fig. S10 A1). This suggests that lipopeptides' direct contact with membranes is not a necessary condition to induce lipid demixing. This suggests that lipopeptide micelles could possibly alter bilayer structure in a way deleterious to cell health even if other components of the microbe's cell surface, such as the lipopolysaccharides, prevented full binding and insertion.

Second, when the micelle associated with the membrane surface, it recruited POPG lipids to stabilize the surface-bound state. The second step is particularly important in order to lower the transition barrier to insertion, because the favorable interactions compensate for the unfavorable exposure of lipopeptide acyl chains to water required for insertion (Fig. 2 A2). This demixing of anionic lipids has been proposed as a separate, pore-independent mechanism for AMP function (54–56).

With the mammalian membrane, there were no favorable long-range interactions to draw the micelle to the membrane surface, so the lipopeptides were instead transferred individually from the micelle into the membrane while the micelle remained more or less undistorted in solution; this situation continued until the micelle became too small to effectively hide the remaining acyl chains, at which point the remaining AMLPs were transferred simultaneously into the membrane. This is the origin of the large barrier to insertion seen in Fig. 2 B2. This can also be seen from the progression of size distribution of lipopeptide clusters where the

diminishing oligomers lingered much longer in the bacterial membrane case than the mammalian membrane case, as is evident by the high-end orange curves shown in Fig. S8 A2 compared to those in Fig. S8 B2. What's more, because the intermediate-size micelles are metastable in water as discussed in Section S4.1 in the *Supporting Material*, the gradual insertion into the mammalian membrane case gave rise to a more rugged free energy landscape, especially around the transition peaks (Figs. 2 B and 3). It is worth mentioning here that even in case of the bacterial membrane, the lipopeptides could be transferred individually from the micelle into the membrane during the transition state but much less significantly so compared to the mammalian case (see Section S5.2 in the *Supporting Material*). This partial insertion is due to the metastability of the whole 48-mer micelle as discussed in Section S4.1 in the *Supporting Material* as well as the presence of the anionic membrane, which absorbed the inserted monomers and stabilized the degraded micelle via favorable electrostatic interactions.

As mentioned above, there was a turning point in the mammalian membrane case where the micelle became small enough such that its insertion into the membrane became cooperative (compare Fig. S7, B1 and B2). The system arrived at a critical point where the barrier to transferring one more lipopeptide into the membrane balanced out that of pushing the entire oligomer into the membrane; at this point, the rest of the lipopeptides went into the membrane together. The size of this intermediate micelle was somewhere between a 20- and a 30-mer, which was around the equilibrium sizes expected in solution (see Figs. 1 and S6 and Section S4.1 in the *Supporting Material*). This raises a very important question regarding the membrane selectivity of AMLPs: if such intermediate micelles are well populated as compared to larger ones, the AMLP's binding to the mammalian membrane via these intermediate micelles could become comparably fast as to the bacterial membrane. If so, one could imagine rationally optimizing the oligomerization state in order to improve selectivity and reduce side effects from damaging host membranes. However, doing so would require us to consider the surface structures of different cell types as they might interact with micelles of a specific range of sizes.

CONCLUSIONS

In this study, we used coarse-grained MD simulations of an antimicrobial lipopeptide to quantify its free energy of oligomerization in solution, as well as the free energy of a typical oligomer's binding to two lipid bilayer compositions, chosen to mimic bacterial and mammalian membranes. Our results indicated that this lipopeptide, C16-KGGK, is polydisperse in solution, with an equilibrium of oligomers of various sizes. While a previous simulation study showed that the monomer binds to any

membrane rapidly and with high affinity (26), this work showed that the oligomer's binding to membranes needed to overcome a significant free energy barrier that varies with membrane composition. The result is enhanced thermodynamic and kinetic selectivity for bacterial versus mammalian model membranes.

This study suggests a possible new variable to consider when rationally optimizing membrane-active peptidic drugs: controlling the oligomeric state in solution will vary the mechanism of binding and thus the binding kinetics in ways not readily predictable by considering the monomer alone. Given the other practical benefits to oligomerization—better solubility, reduced vulnerability to proteolysis, etc.—this insight may help lead to better antibiotics based on AMPs.

SUPPORTING MATERIAL

Supporting Materials and Methods, Supporting Results, eleven figures, and one table are available at [http://www.biophysj.org/biophysj/supplemental/S0006-3495\(15\)00717-1](http://www.biophysj.org/biophysj/supplemental/S0006-3495(15)00717-1).

AUTHOR CONTRIBUTIONS

D.L. and A.G. designed the research; D.L. performed the research; D.L. contributed analytic tools; D.L. analyzed the data; and D.L. and A.G. wrote the article.

ACKNOWLEDGMENTS

We thank the Center for Integrated Research Computing at the University of Rochester for providing computational resources in our research.

This work was supported by grant No. GM095496 from the National Institutes of Health, Bethesda, MD.

REFERENCES

- Koczulla, A. R., and R. Bals. 2003. Antimicrobial peptides: current status and therapeutic potential. *Drugs*. 63:389–406.
- Jenssen, H., P. Hamill, and R. E. W. Hancock. 2006. Peptide antimicrobial agents. *Clin. Microbiol. Rev.* 19:491–511.
- Piddock, L. J. V. 2006. Multidrug-resistance efflux pumps—not just for resistance. *Nat. Rev. Microbiol.* 4:629–636.
- Lomovskaya, O., H. I. Zgurskaya, ..., W. J. Watkins. 2007. Waltzing transporters and ‘the dance macabre’ between humans and bacteria. *Nat. Rev. Drug Discov.* 6:56–65.
- Hancock, R. E. W., and H.-G. Sahl. 2006. Antimicrobial and host-defense peptides as new anti-infective therapeutic strategies. *Nat. Biotechnol.* 24:1551–1557.
- Straus, S. K., and R. E. W. Hancock. 2006. Mode of action of the new antibiotic for Gram-positive pathogens daptomycin: comparison with cationic antimicrobial peptides and lipopeptides. *Biochim. Biophys. Acta*. 1758:1215–1223.
- Oren, Z., J. C. Lerman, ..., Y. Shai. 1999. Structure and organization of the human antimicrobial peptide LL-37 in phospholipid membranes: relevance to the molecular basis for its non-cell-selective activity. *Biochem. J.* 341:501–513.

8. Raimondo, D., G. Andreotti, ..., A. Scaloni. 2005. A folding-dependent mechanism of antimicrobial peptide resistance to degradation unveiled by solution structure of distinctin. *Proc. Natl. Acad. Sci. USA.* 102:6309–6314.
9. Strahilevitz, J., A. Mor, ..., Y. Shai. 1994. Spectrum of antimicrobial activity and assembly of dermaseptin-b and its precursor form in phospholipid membranes. *Biochemistry.* 33:10951–10960.
10. Ghosh, J. K., D. Shaool, ..., A. Mor. 1997. Selective cytotoxicity of dermaseptin S3 toward intraerythrocytic *Plasmodium falciparum* and the underlying molecular basis. *J. Biol. Chem.* 272:31609–31616.
11. Oren, Z., and Y. Shai. 2000. Cyclization of a cytolytic amphipathic α -helical peptide and its diastereomer: effect on structure, interaction with model membranes, and biological function. *Biochemistry.* 39:6103–6114.
12. Feder, R., A. Dagan, and A. Mor. 2000. Structure-activity relationship study of antimicrobial dermaseptin S4 showing the consequences of peptide oligomerization on selective cytotoxicity. *J. Biol. Chem.* 275:4230–4238.
13. Kustanovich, I., D. E. Shalev, ..., A. Mor. 2002. Structural requirements for potent versus selective cytotoxicity for antimicrobial dermaseptin S4 derivatives. *J. Biol. Chem.* 277:16941–16951.
14. Sal-Man, N., Z. Oren, and Y. Shai. 2002. Preassembly of membrane-active peptides is an important factor in their selectivity toward target cells. *Biochemistry.* 41:11921–11930.
15. Fjell, C. D., J. A. Hiss, ..., G. Schneider. 2012. Designing antimicrobial peptides: form follows function. *Nat. Rev. Drug Discov.* 11:37–51.
16. Neale, C., J. C. Y. Hsu, ..., R. Pomès. 2014. Indolicidin binding induces thinning of a lipid bilayer. *Biophys. J.* 106:L29–L31.
17. Romo, T. D., and A. Grossfield. 2014. Unknown unknowns: the challenge of systematic and statistical error in molecular dynamics simulations. *Biophys. J.* 106:1553–1554.
18. Avrahami, D., and Y. Shai. 2003. Bestowing antifungal and antibacterial activities by lipophilic acid conjugation to D,L-amino acid-containing antimicrobial peptides: a plausible mode of action. *Biochemistry.* 42:14946–14956.
19. Avrahami, D., and Y. Shai. 2004. A new group of antifungal and antibacterial lipopeptides derived from non-membrane active peptides conjugated to palmitic acid. *J. Biol. Chem.* 279:12277–12285.
20. Makovitzki, A., D. Avrahami, and Y. Shai. 2006. Ultrashort antibacterial and antifungal lipopeptides. *Proc. Natl. Acad. Sci. USA.* 103:15997–16002.
21. Vallon-Eberhard, A., A. Makovitzki, ..., Y. Shai. 2008. Efficient clearance of *Aspergillus fumigatus* in murine lungs by an ultrashort antimicrobial lipopeptide, palmitoyl-lys-ala-D-Ala-lys. *Antimicrob. Agents Chemother.* 52:3118–3126.
22. Papo, N., Z. Oren, ..., Y. Shai. 2002. The consequence of sequence alteration of an amphipathic α -helical antimicrobial peptide and its diastereomers. *J. Biol. Chem.* 277:33913–33921.
23. Makovitzki, A., J. Baram, and Y. Shai. 2008. Antimicrobial lipopolypeptides composed of palmitoyl di- and tricationic peptides: in vitro and in vivo activities, self-assembly to nanostructures, and a plausible mode of action. *Biochemistry.* 47:10630–10636.
24. Horn, J. N., T. D. Romo, and A. Grossfield. 2013. Simulating the mechanism of antimicrobial lipopeptides with all-atom molecular dynamics. *Biochemistry.* 52:5604–5610.
25. Horn, J. N., J. D. Sengillo, ..., A. Grossfield. 2012. Characterization of a potent antimicrobial lipopeptide via coarse-grained molecular dynamics. *Biochim. Biophys. Acta.* 1818:212–218.
26. Lin, D., and A. Grossfield. 2014. Thermodynamics of antimicrobial lipopeptide binding to membranes: origins of affinity and selectivity. *Biophys. J.* 107:1862–1872.
27. Rzepiela, A. J., D. Sengupta, ..., S. J. Marrink. 2010. Membrane poration by antimicrobial peptides combining atomistic and coarse-grained descriptions. *Faraday Discuss.* 144:431–481.
28. Louhivuori, M., H. J. Risselada, ..., S. J. Marrink. 2010. Release of content through mechano-sensitive gates in pressurized liposomes. *Proc. Natl. Acad. Sci. USA.* 107:19856–19860.
29. Marrink, S. J., A. H. de Vries, and A. E. Mark. 2004. Coarse grained model for semiquantitative lipid simulations. *J. Phys. Chem. B.* 108:750–760.
30. Marrink, S. J., H. J. Risselada, ..., A. H. de Vries. 2007. The MARTINI force field: coarse grained model for biomolecular simulations. *J. Phys. Chem. B.* 111:7812–7824.
31. Risselada, H. J., and S. J. Marrink. 2008. The molecular face of lipid rafts in model membranes. *Proc. Natl. Acad. Sci. USA.* 105:17367–17372.
32. Singh, G., and D. P. Tieleman. 2011. Using the Wimley-White hydrophobicity scale as a direct quantitative test of force fields: the MARTINI coarse-grained model. *J. Chem. Theory Comput.* 7:2316–2324.
33. Monticelli, L., D. P. Tieleman, and P. F. J. Fuchs. 2010. Interpretation of ^2H -NMR experiments on the orientation of the transmembrane helix WALP23 by computer simulations. *Biophys. J.* 99:1455–1464.
34. Castillo, N., L. Monticelli, ..., D. P. Tieleman. 2013. Free energy of WALP23 dimer association in DMPC, DPPC, and DOPC bilayers. *Chem. Phys. Lipids.* 169:95–105.
35. Kasson, P. M., N. W. Kelley, ..., V. S. Pande. 2006. Ensemble molecular dynamics yields submillisecond kinetics and intermediates of membrane fusion. *Proc. Natl. Acad. Sci. USA.* 103:11916–11921.
36. Yesylevskyy, S. O., L. V. Schäfer, ..., S. J. Marrink. 2010. Polarizable water model for the coarse-grained MARTINI force field. *PLOS Comput. Biol.* 6:e1000810.
37. de Jong, D. H., G. Singh, ..., S. J. Marrink. 2013. Improved parameters for the MARTINI coarse-grained protein force field. *J. Chem. Theory Comput.* 9:687–697.
38. Serrano, G. N., G. G. Zhanel, and F. Schweizer. 2009. Antibacterial activity of ultrashort cationic lipo- β -peptides. *Antimicrob. Agents Chemother.* 53:2215–2217.
39. Kumar, S., J. M. Rosenberg, ..., P. A. Kollman. 1992. The weighted histogram analysis method for free-energy calculations on biomolecules. I. The method. *J. Comput. Chem.* 13:1011–1021.
40. Chodera, J. D., and M. R. Shirts. 2011. Replica exchange and expanded ensemble simulations as Gibbs sampling: simple improvements for enhanced mixing. *J. Chem. Phys.* 135:194110.
41. Grossfield, A. WHAM: an implementation of the weighted histogram analysis method. Ver. 2.0.5. <http://membrane.urmc.rochester.edu/content/wham/>.
42. Zhu, F., and G. Hummer. 2012. Convergence and error estimation in free energy calculations using the weighted histogram analysis method. *J. Comput. Chem.* 33:453–465.
43. Press, W. H., S. A. Teukolsky, ..., B. P. Flannery. 2007. Numerical Recipes: The Art of Scientific Computing, 3rd Ed. Cambridge University Press, New York.
44. Holoborodko, P. 2008–2014. MPFR C++. <http://www.holoborodko.com/pavel/mpfr/>.
45. Lin, D. GWHAM: a C++ implementation of generalized weighted histogram analysis method. <https://github.com/dejunlin/gwham>.
46. E, W., W. Ren, and E. Vanden-Eijnden. 2007. Simplified and improved string method for computing the minimum energy paths in barrier-crossing events. *J. Chem. Phys.* 126:164103.
47. Hess, B., C. Kutzner, ..., E. Lindahl. 2008. GROMACS 4: algorithms for highly efficient, load-balanced, and scalable molecular simulation. *J. Chem. Theory Comput.* 4:435–447.
48. van der Spoel, D., E. Lindahl, ..., H. J. C. Berendsen. 2005. GROMACS: fast, flexible, and free. *J. Comput. Chem.* 26:1701–1718.
49. Pronk, S., S. Páll, ..., E. Lindahl. 2013. GROMACS 4.5: a high-throughput and highly parallel open source molecular simulation toolkit. *Bioinformatics.* 29:845–854.

50. Nose, S., and M. L. Klein. 1983. Constant pressure molecular dynamics for molecular systems. *Mol. Phys.* 50:1055–1076.
51. Hoover, W. G. 1985. Canonical dynamics: equilibrium phase-space distributions. *Phys. Rev. A.* 31:1695–1697.
52. Parrinello, M., and A. Rahman. 1981. Polymorphic transitions in single crystals: a new molecular dynamics method. *J. Appl. Phys.* 52:7182–7190.
53. Melo, M. N., R. Ferre, and M. A. R. B. Castanho. 2009. Antimicrobial peptides: linking partition, activity and high membrane-bound concentrations. *Nat. Rev. Microbiol.* 7:245–250.
54. Epand, R. M., and R. F. Epand. 2009. Lipid domains in bacterial membranes and the action of antimicrobial agents. *Biochim. Biophys. Acta.* 1788:289–294.
55. Epand, R. F., L. Maloy, ..., R. M. Epand. 2010. Amphipathic helical cationic antimicrobial peptides promote rapid formation of crystalline states in the presence of phosphatidylglycerol: lipid clustering in anionic membranes. *Biophys. J.* 98:2564–2573.
56. Epand, R. M., and R. F. Epand. 2011. Bacterial membrane lipids in the action of antimicrobial agents. *J. Pept. Sci.* 17:298–305.